

A Temperature Model of the Crust beneath the Barents Sea: Investigations along Geotraverses

M. D. Khutorskoi^a, K. G. Viskunova^b, L. V. Podgornykh^b,
O. I. Suprunenko^b, and V. R. Akhmedzyanov^a

^a*Geological Institute, Russian Academy of Sciences, Pyzhevskii per. 7, Moscow, 119017 Russia*

e-mail: mkhutorskoy@ginras.ru

^b*All-Russia Research Institute of Geology and Mineral Resources of the World Ocean, Angliiskii pr. 1, St. Petersburg, 190121 Russia*

Received September 14, 2006

Abstract—2D and 3D modeling of the geothermal field was carried out along seven extended geotraverses in the Barents Sea compiled on the basis of CMP profiling and results of deep drilling. Depths of the zone characterized by catagenetic transformation of organic matter were calculated for different areas of the sedimentary basin. The minimal depth is confined to the South Barents Basin with the highest hydrocarbon resource potential established by geological exploration. In 3D models, this area is distinguished by a thermal dome recognized for the first time.

DOI: 10.1134/S0016852108020039

INTRODUCTION

The geological and economic significance of the Arctic seas is due to the large petroleum resources of shelf sedimentary basins. With the development of known oil and gas fields and the discovery of new ones, the significance of the Arctic seas will progressively increase.

Under conditions of limited investments in conducting expensive geological and geophysical surveying and high risks of exploration on shelves, relatively inexpensive, indirect high-end methods of assessment of hydrocarbon resource potential that are based on available geological and geophysical data have important practical implications.

The data obtained along extended geotraverses based on the results of CMP profiling and drilling offer wide opportunities for the application of new technologies to the study of the geological structure and forecasting hydrocarbon resources in sedimentary basins.

We performed geothermal modeling along geotraverses in the Barents Sea to determine the temperature in the Earth's crust, to estimate the depth of zones characterized by different degrees of catagenetic transformation of organic matter, and to study characteristic manifestations of the geothermal field that control localization of the known gas and gas-condensate fields.

GEOHERMAL STUDIES IN THE BARENTS SEA: THE STATE OF THE ART

The geothermal studies on the shelf of the Eurasia Basin in the Arctic Ocean started in the Barents Sea

with measurements by submersible PTG sounds in the 1970s [6]. The first measurements were made on the shelf at a water depth above 300 m with penetration of one-channel sound into sediments down to a depth of 2 m. The results obtained demonstrated the expected strong effect of exogenic thermal fields on the terrestrial heat flow, which was subjected to the effect of seasonal temperature oscillations at the sea bottom that are due to insolation and bottom currents that supplied water at contrasting (relative to the background) temperatures. This factor is particularly notable in the southern part of the sea affected by the warm Nordkapp Current. In this context, the measurements implemented without special processing based on the knowledge of seasonal temperature fluctuations prevented obtainment of conditional assessments of the background terrestrial heat flow because the range of measured values was very wide (from 0 to 500 mW/m²) and did not adequately reflect the distribution of deep thermal sources.

The intense exploration for oil and gas fields in shelf basins that commenced in the 1980s included offshore and deep drilling on islands accompanied by thermal logging. In addition, the first measurements of the heat flow in wells were performed at that time in the southern Kara Sea. In the 1980s–1990s, the measurements of heat flow by submersible sounds were performed in the central and southeastern Barents Sea [2, 5] and the empirical data were subsequently processed with allowance for seasonal bottom-temperature fluctuations [12]. The processing of thermal measurements made it possible to estimate thermal gradients, while thermophysical studies of drill cores resulted in mea-

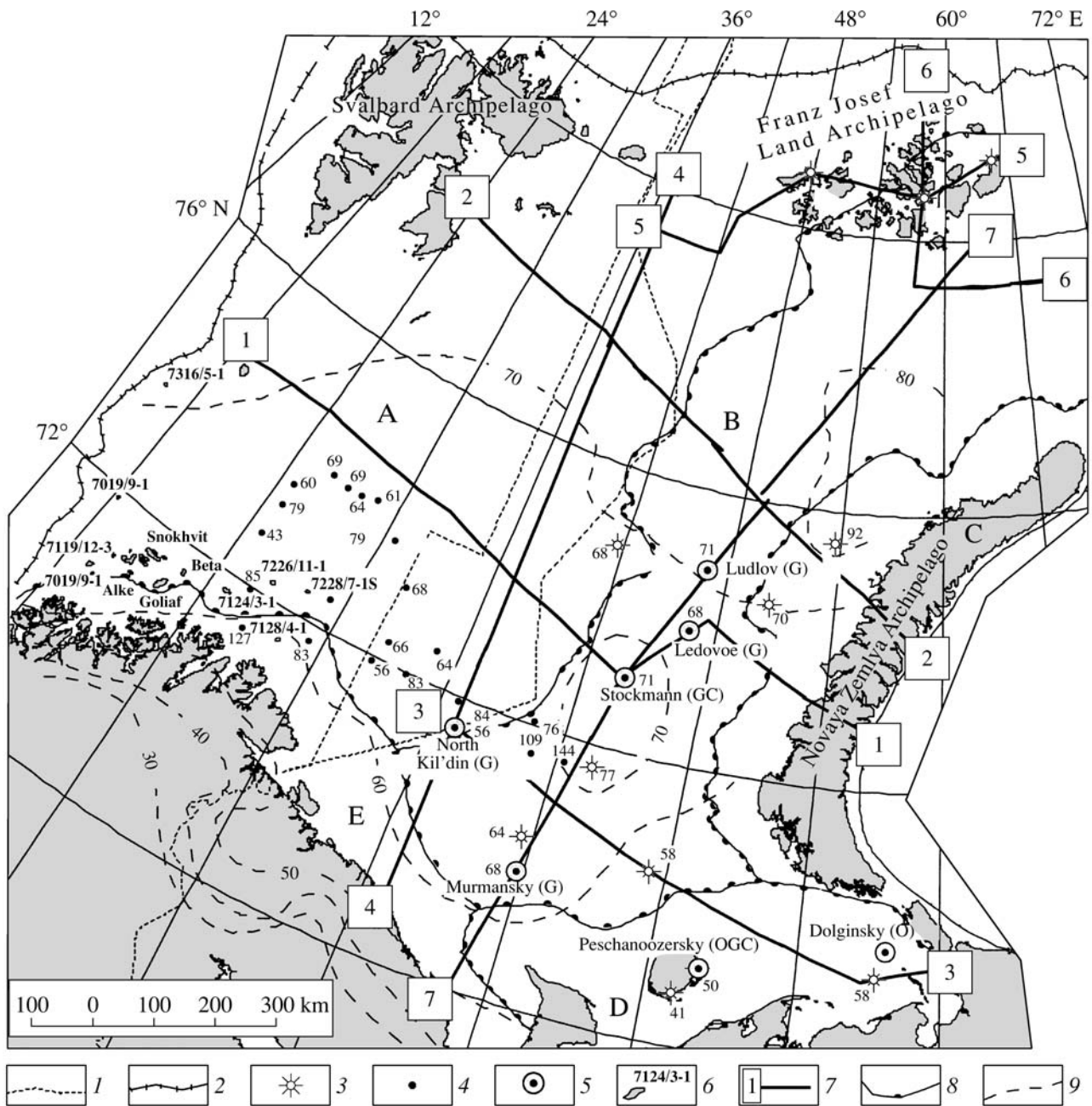


Fig. 1. Map of the heat flow density in the Barents Sea region and adjacent areas. (1) Border of Russia and median line (according to the proposal of Norway of 1970); (2) shelf edge; (3) deep well; (4) station of heat-flow measurements and its value, mW/m^2 ; (5) petroleum fields in the Russian sector; (6) the same in the Norwegian sector; (7) line of seismic and geological profile and its number; (8) boundaries of regional tectonic elements; (9) contour line of heat flow, mW/m^2 . Tectonic elements (letters in figure): (A) Svalbard Plate, (B) East Barents Megatrough, (C) Pai-Khoi-Novaya Zemlya Fold System, (D) Pechora Plate, (E) Kola Homocline. Fluid type: (G) gas, (GC) gas condensate, (OGC) oil-gas condensate, (O) oil.

surement of the heat conductivity of rocks. These works provided the first conditional values of heat flow in the region under consideration [21], which were subsequently specified by Levashkevich [5] (Fig. 1). However, the geothermal measurements in wells were sparse and insufficient for adequate mapping of the temperature and heat flow distribution in such a vast

territory, especially for calculating deep temperatures in the lithosphere.

Nevertheless, the analysis of available data obtained by measurements in wells and thermal sounding revealed a tendency for an increase in heat flow in the northeastern and northwestern directions. For example, in the zone of conjugation of the Kola microplate and

the Baltic Shield, the heat flow averages 54 mW/m^2 and amounts to 70 mW/m^2 in the North Barents Basin and Central Barents Uplift. To a first approximation, such a trend in heat-flow variations can be explained by approaching the North Atlantic spreading center, where the thermal activity of the asthenosphere increases. At the same time, our data indicate that the crust of the Barents Plate is subjected to secondary processes, which become younger in the northern direction. On the basis of interpretation of geothermal data, it was suggested that the secondary thermal processes are related to rifting [19].

Modeling of the nonstationary thermal field in order to calculate deep temperatures and heat flows was performed along each of the profiles shown in Fig. 1.

The geotraverses extend via the wells, where the conditional heat flow measurements were conducted. Such measurements made it possible to correctly set the Neumann (second-type) boundary conditions at the lower margin of each profile.

Initial conditions for temperature calculation were set for 60 Ma ago. As follows from paleotectonic reconstructions for the Barents Sea [1, 15], the present-day structure of the crust was already formed by that time. Therefore, the evolution of the thermal field, if it occurred, was related to relaxation of initial thermal heterogeneities rather than to the reorganization of structural and thermophysical elements.

Under such boundary and initial conditions, the temperature within the modeling region is rapidly coming to a steady state, which was a priori accepted as a criterion of calculation correctness. The duration of time steps was 10 Ma. Thus, six control stages were taken over the time interval of 60 Ma to verify the stationary state. The modeling has shown that, since the third step, i.e., 30 Ma after the onset of calculation, all the profiles are characterized by a steady-state thermal field.

GEOLOGICAL SECTIONS ALONG GEOTRAVERSES

The age of the sedimentary cover of the Barents Sea region comprises the time interval from the Vendian (?)–Cambrian to the Cenozoic. The sedimentary rocks of these ages, especially pre-Cenozoic, are observable mainly at the periphery of the Barents Sea shelf (on islands and seashores) and as cores of sparse reference parametric wells on islands and offshore prospecting and exploratory wells drilled in the Russian sector of the sea. The Norwegian sector of the Barents Sea, located west of Profile 4–4 (Fig. 1), is studied much better by drilling and seismic surveying.

The geological sections presented in Figs. 2–6 are based on the data obtained from the CMP surveying carried out by the Marine Arctic Geological Exploration Expedition, the results of drilling in the Russian sector performed by the Arctic Marine Petroleum Exploration Expedition, and the published drilling

results in the Norwegian sector. The land segments of the sections were compiled on the basis of the data obtained through geological mapping by teams from the All-Russia Research Institute of Geology and Mineral Resources of the World Ocean and the Polar Marine Geological Exploration Expedition.

The sections cross the main tectonic elements of the Barents Sea region and characterize the regional structure of the sedimentary cover. Its maximal thickness (~18 km) was recorded in the South Barents Basin (Fig. 1, profiles 1–1, 2–2, 3–3, and 7–7). The minimal thickness is confined to the western Barents Sea region in the Norwegian sector (profiles 1–1 and 2–2). Profile 4–4, which extends in the meridional direction, crosses the zone of the Central Barents uplifts separated by troughs that open into the South Barents Basin.

The Cretaceous; Jurassic; Upper, Middle, and, partly, Lower Triassic sediments were reduced in the Norwegian sector owing to the Late Cretaceous–Eocene uplifting. The most complete Mesozoic sections are recorded in depocenters of the South and North Barents basins.

According to CMP seismic data, the sedimentary cover of these areas is composed (from the bottom upward) of the Ordovician–Silurian, Devonian, Carboniferous, and Lower Permian deepwater formations, which grade higher into the largely terrigenous Upper Permian, Triassic, Jurassic, Cretaceous, and Cenozoic sequences.

The Mesozoic part of the well sections is characterized by alternation of transgressive and regressive successions. The peak of transgression fell on the Late Jurassic when the so-called black clay was deposited [14]. The deepest well drilled in this part of the region—the Arctic-1 Well—was stopped in the Ladinian sediments (Middle Jurassic) at a depth of 4524 m.

The wells drilled in the Murmansk area in marginal parts of the South Barents Basin demonstrate a substantial decrease in the thickness of Triassic and older sediments and the absence of the Upper Cretaceous strata. According to CMP data, they are underlain by Lower Permian, Carboniferous, and Upper Devonian carbonate rocks (Fig. 1, Profile 7–7) similar to those in the northern Timan–Pechora Plate.

In the Pechora Sea, the Paleozoic rocks are penetrated by prospecting and exploratory wells. Well 1 drilled in the Gulyaevsky field and wells 1–5 in the Prirazlomny field are located in the immediate proximity to Profile 3–3. Well 5 penetrated the sedimentary cover down to a depth of 4500 m and was stopped in the basal unit of the Lower Devonian. It was established that the Paleozoic sedimentary rocks of the Pechora Sea, including the main Carboniferous–Lower Permian petroliferous complex, have many features in common with the section in the onshore part of the province [3].

Profiles 5–5 and 6–6 are located in the northernmost part of the Barents Sea Megabasin and cross some islands of the Franz Josef Land Archipelago and the

Thermophysical parameters accepted for modeling of the geothermal field in the Earth's crust

Rocks	Boundary seismic velocity, km/s	Thermal diffusivity, $a \times 10^{-7}$, m ² /s	Thermal conductivity, k , W/(m K)	Heat generation (norm.), $Fi \times 10^{-13}$ K/s
Nonlithified sediments	<3.7	3.0	1.3	–
Lithified Mesozoic–Cenozoic sediments		3.5	1.5	–
Paleozoic carbonate sediments	4.7	3.8	1.9	1.5
Granites	Upper part	6.0	5.0	5.52
	Lower part	6.5	5.0	3.5
Basalts, rocks of crust–mantle mixture	>6.5	7.0	2.9	–
Crustal ultramafics	–	8.0	3.0	–
Mantle ultramafics	–	10.0	3.2	–

adjacent areas (Fig. 1). The sections are based on the data of geological mapping and the Nagursky, Northern, and HEIS deep wells. The sharp variations in thickness and the absence of pre-Triassic sediments in most areas of the archipelago have been documented. Numerous intrusive bodies in the Triassic sequence are crossed by wells and recorded in CMP seismic sections. In the Nagursky Well, the Triassic rocks are underlain by the Upper Carboniferous sequence. The more continuous Permian, Carboniferous, Devonian, and Silurian sequences are suggested to occur in the troughs, where the total thickness of the sedimentary cover increases up to 6 km. According to CMP data, offshore parts of sections are assumed to include also Jurassic and Cretaceous sediments. Inasmuch as profiles 5–5 and 6–6 (Fig. 1) are not representative for geothermal modeling, they are omitted in this paper.

TECHNIQUE OF GEOTHERMAL MODELING

To estimate temperatures at the depths that are not accessed by drilling and to define the temperature boundaries in the lithosphere corresponding to zones of oil and gas generation, a technique of 2D and 3D modeling of the nonstationary thermal field was developed. The thermophysical medium, i.e., the configuration of contrasting thermophysical layers and values of thermal conductivity and diffusivity, were set by corresponding digitizing structural complexes along geotraverses recognized on the basis of seismic and geological data. The thermophysical parameters adequate for the established boundary seismic velocities or lithological characteristics of rocks penetrated by wells were used in calculations (table).

The temperature at deep well bottoms (Dirichlet, or first-type boundary conditions) or the heat flow measured in the deepest wells (Neumann, or second-type boundary conditions) were used as conditions at the lower boundary of the modeling region. The average annual temperature at the Earth's surface is accepted as a condition at the upper boundary of the modeling region that is commonly limited from above by the

Earth's surface, or more exactly, by a neutral layer level. The condition of zero horizontal outflow of heat, i.e. $\partial T/\partial x = 0$, is met at lateral boundaries.

In this study, the Neumann boundary conditions were always set at the lower margin of the modeling region.

The calculation of deep temperature along each profile were performed with the original TERMOGRAF program packet [15].

The numerical method of finite elements with a square approximation of the temperature function between nodes of a rectangular grid was used to establish the temperature distribution through the section. A grid of 41×41 nodes is provided in the program; i.e., the two-dimensional problem is solved. Linear dimensions of the node along the X and Z axes are changeable at the will of the operator. Configuration of contrasting media and their thermophysical parameters, such as thermal diffusivity a (m²/s), thermal conductivity k (W/(m K)), and normalized density of heat sources $Q/(c\rho)$ (K/s), were preset within the modeling region. The linear dimensions (L_x and L_z , km) of the modeling region, which define the linear dimensions of a node ($L_x/41$ and $L_z/41$), as well as the time interval of solution quantization (Ma), were set in the computing complex. The temporal step of the iteration is selected automatically by the program and calculated according to the Courant criterion as $\tau = 10^{-7}(Z^2/4a)$, where Z is the thickness of the modeling region.

The numerical solution of the thermal conductivity equation

$$\left(k_x \frac{\partial^2 T}{\partial x^2} + k_z \frac{\partial^2 T}{\partial z^2} \right) + A(x, z) = c\rho \frac{\partial T}{\partial \tau}, \quad (1)$$

where k , c , and ρ are the thermal conductivity, heat capacity, and density of lithospheric layers, respectively; $A(x, z)$ is the density of heat sources in the layer; and τ is the time, yields the distribution of temperatures and heat flows $q(z)$ and $q(x)$ for the accepted thermophysical medium at a finite moment of the temporal discretization. The obtained resultant file is renamed as the

file of initial temperatures, and calculation at the next stage starts from the last moment of the previous stage. The possibility of solution discretization is convenient when the necessity arises to change the thermophysical medium in connection with the independently established structural or lithological rearrangements of the geological section, to set the distribution of new sources and heat sinks, and to browse the results of the paleotemperature field calculation. When the heat and mass transfer should be set in the model, it can be simulated via setting of the boundary temperature and/or the adiabatic gradient in the depth interval involved in convection.

During modeling, the following parameters were set for each profile: (i) the temperature at the upper boundary based on meteorological data and (ii) the heat flow at the lower boundary (q_{bound}), which corresponds to the value measured in the nearest wells (q_{obs}) minus the heat flow generated in the crust above the lower boundary of the modeling region owing to the spontaneous decay of long-living radioisotopes (q_{rad}), i.e.,

$$q_{\text{bound}} = q_{\text{obs}} - q_{\text{rad}}$$

The resultant heat flow is calculated from the seismic data on the layer thickness (z_i), the layer's composition, and commonly adopted specific heat generation $A(x, z)$ for a respective rock type: $(q_{\text{rad}})_i = A(x, z)z_i$ [10].

The calculation accuracy was assessed according to two criteria: (1) coincidence of model and measured heat flows in wells and (2) coincidence of temperatures at the intersection of profiles.

The modeling was performed in 2D and 3D geometry. The 3D regional geothermal model was developed with the TECPLOT ver. 7.0 program packet (Amtec Engineering Inc.) for 3D graphics, which provides volumetric interpretation of the observed field (temperature, heat flow, and structural seismotomographic boundaries) in latitude–longitude–depth coordinates. For preparing data files in the TECPLOT ver. 7.0 format, a special original program was written. This program transforms the text file with the results of thermal modeling into the TECPLOT database format, while coordinates of the beginning and end of the profile and discretization of depth intervals are set. The TECPLOT program provides for the 3D interpolation in a grid of any configuration. The irregular grid coordinated with directions of seismic profiles, along which the 2D distribution of deep temperatures was calculated, was used in most cases. Thus, equation (1) is supplemented by

the third missing derivative $\left(k_y \frac{\partial^2 T}{\partial y^2}\right)$ and turns into the

3D equation of heat conductivity. The results of calculating the temperature field by means of interpolation approximation differ from the results obtained by solution of the direct problem for a 3D medium only by a distortion caused by perturbation of the heat flow along the Y axis. The long-term experience in 2D thermal

modeling shows, however, that this value is negligible. For example, the heat flow along the Y axis in a typical sedimentary basin does not exceed 0.04 mW/m^2 , i.e., is three orders of magnitude lower than the background terrestrial heat flow. Hence, the 3D temperature distribution obtained from volumetric interpolation is practically adequate for the solution of the direct problem for the volumetric thermal field.

2D TEMPERATURE MODELS OF GEOTRAVERSES

The western segment of Profile 1–1 extends in the near-latitudinal direction in the central part of the Barents Sea from Medvezhii Island to the Stockmann–Lunin Threshold (Fig. 2). As elsewhere, the boundaries between the Proterozoic basement and the Phanerozoic sedimentary cover and between the Upper Paleozoic carbonate complex and the Mesozoic–Cenozoic terrigenous rocks are the main thermophysical boundaries along this profile. The structural and thermophysical heterogeneities along the geothermal geotraverse are emphasized by curved isotherms and an elevated geothermal gradient in relatively low-conductivity sequences. For example, the temperature gradient in the depth interval of 5–10 km changes from 12–14 to 20–21 mK/m in the folded basement and Upper Paleozoic cover, respectively. During invariance of the heat flow at the lower boundary of the section, the contrast in gradients is compensated by the reversed relation of thermal conductivities. Therefore, the heat flow along this profile is virtually constant and equal to 68 mW/m^2 .

The temperature interval of $140\text{--}180^\circ\text{C}$ is considered, with some reservations, the bottom of the main zone of oil generation, or an “oil window.” This temperature interval corresponds to depths of 5.0–6.5 and 6–8 km in the eastern and western segments of the profile, respectively. Thus, the geothermal data provide independent evidence for a higher hydrocarbon resource potential of the South Barents Basin relative to that of the Central Barents uplifts [4].

The Profile 2–2 extends northerly parallel to Profile 1–1 from Edge Island of the Svalbard Archipelago to Severnyi Island of the Novaya Zemlya Archipelago to cross the Malygin and Lunin saddles, Admiralty Uplift, and Sedov Trough (Fig. 3).

The most distinct refractions of the terrestrial heat flow along this geotraverse are recorded on the western slope of the Lunin Saddle and in the junction zone between the Sedov Trough and Novaya Zemlya Archipelago. This result is explained not only by structural and thermophysical heterogeneities but also by a lowered heat flow in the Novaya Zemlya area. The heat flow decreases here¹ to 40 mW/m^2 probably owing to the same circumstance as in the Urals, i.e., screening of

¹ The decrease in heat flow in the Novaya Zemlya area is recorded also in the eastern segment of Profile 1–1, which is omitted because of the limited volume of this paper.

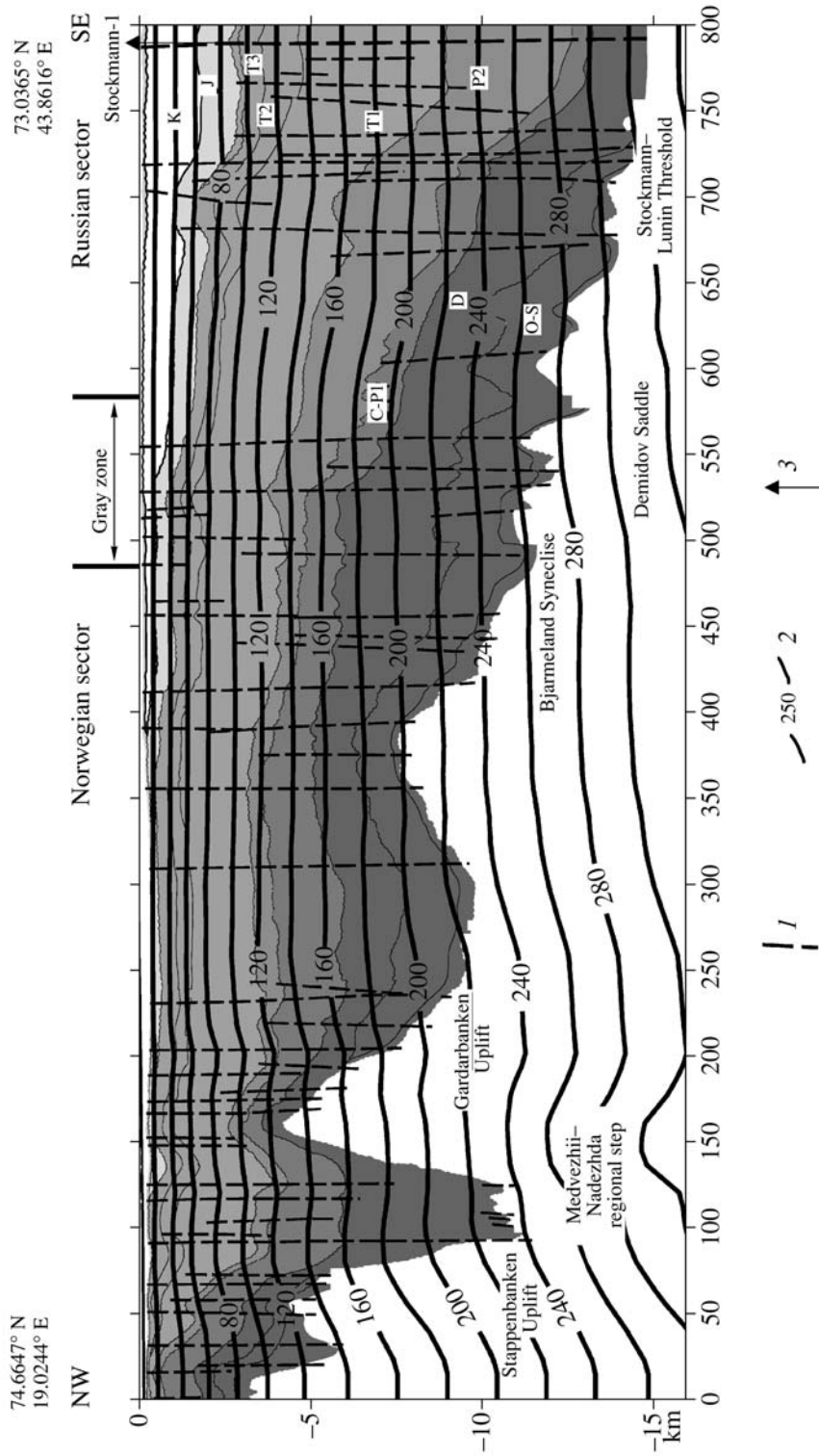


Fig. 2. Geological and geothermal section along Profile 1-1. See Fig. 1 for the profile location. (1) Fault; (2) temperature contour line, °C; (3) deep well. Temperature interval of organic matter catagenesis is bracketed by isotherms of 140 and 180°C.

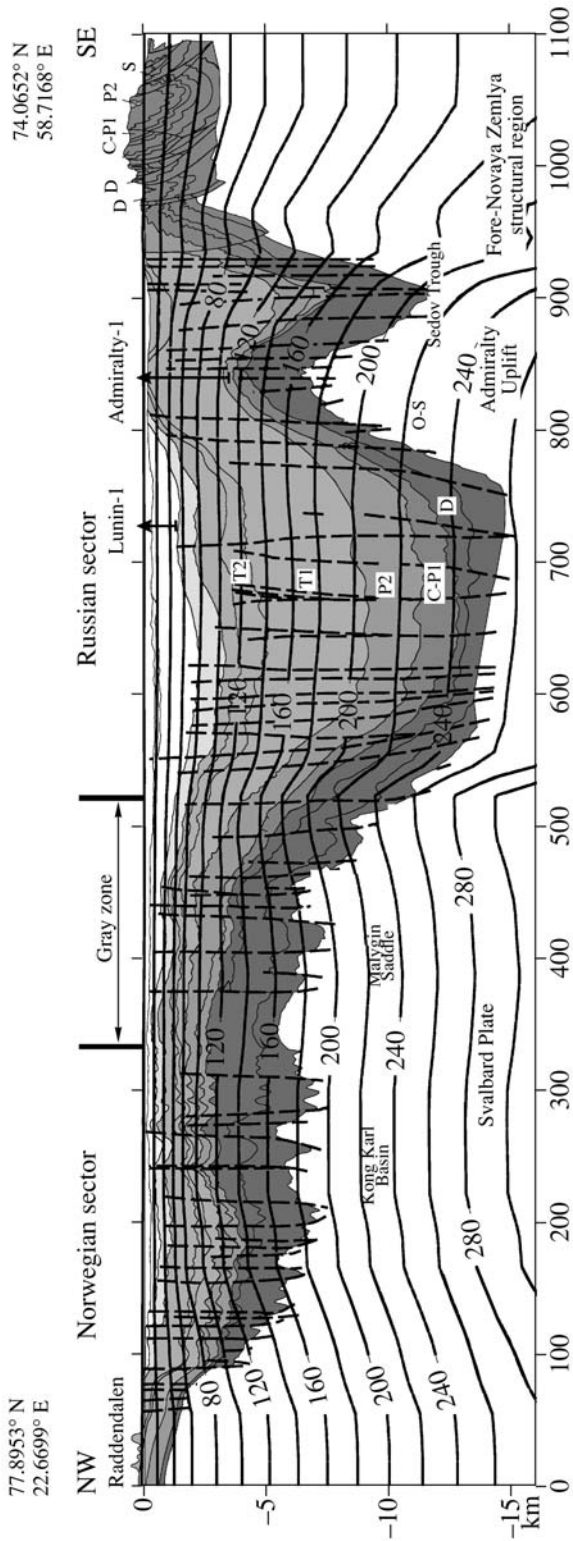


Fig. 3. Geological and geothermal section along Profile 2-2. See Fig. 1 for the profile location and Fig. 2 for the legend.

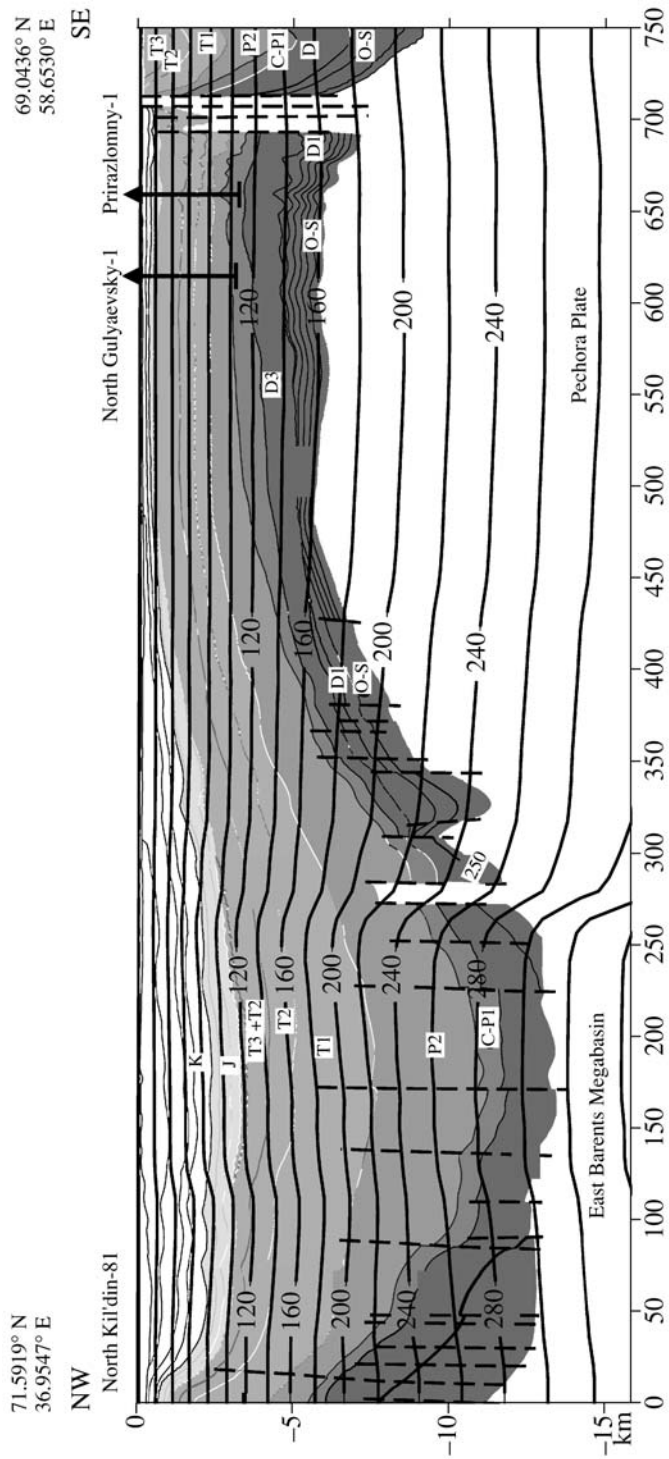


Fig. 4. Geological and geothermal section along Profile 3-3. See Fig. 1 for the profile location and Fig. 2 for legend.

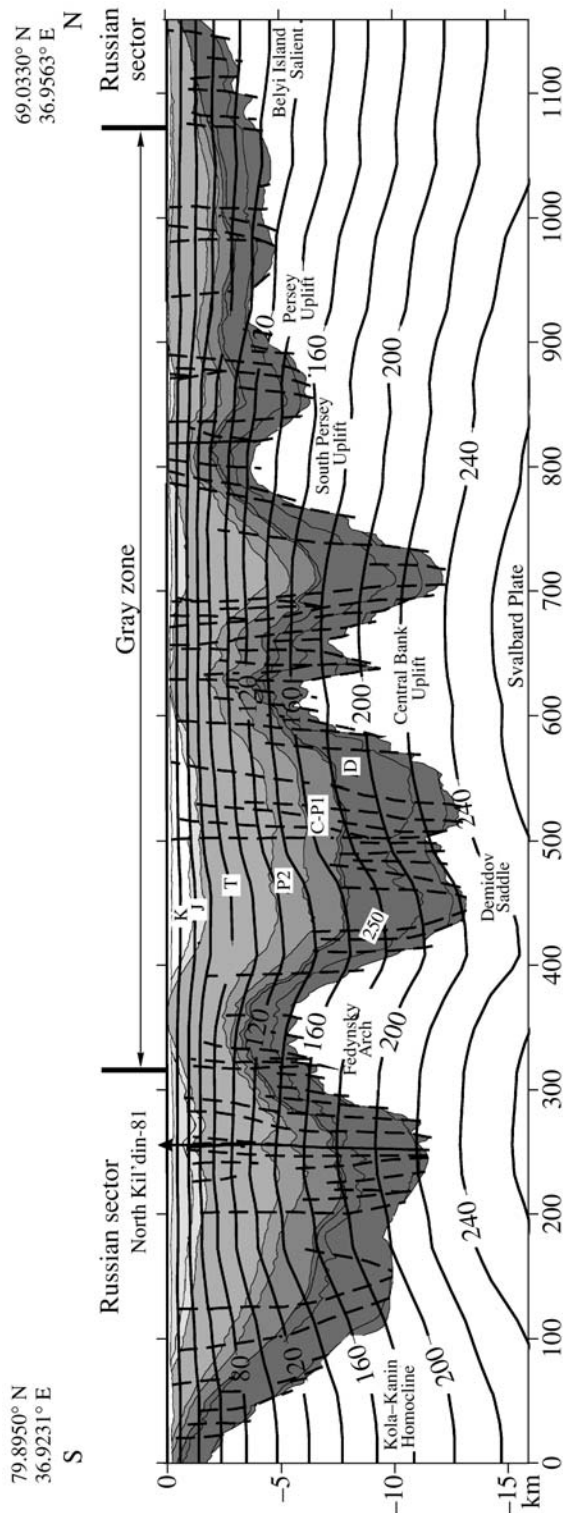


Fig. 5. Geological and geothermal section along Profile 4-4. See Fig. 1 for the profile location and Fig. 2 for legend.

the terrestrial heat flow by the allochthonous lithospheric sheet that was thrust from the paleocean during its closure in the Late Paleozoic [16]. The cooling of the

crust in the eastern segment of the profile caused subsidence of the catagenetic temperature interval from 5–7 km in the Malygin and western Lunin basins to 8–10 km in the Sedov Trough.

Profile 3–3 crosses the Pechora Sea, the most productive part of the Barents Sea Basin, and extends farther eastward via the South Barents Basin to the North Kil'din Well (Fig. 4).

The highest geothermal gradient is established in the South Barents Basin (up to 20–22 mK/m within a depth interval of 5–10 km) owing to the thick low-conductivity Mesozoic–Cenozoic terrigenous complex. As a result, the temperature in the sedimentary cover increases rapidly downward. A temperature of 140°C is recorded in this area at a depth of 4.5 km. Thus, according to the geothermal data, the South Barents Basin is the most promising structural unit with respect to hydrocarbon generation.

Profile 4–4 extends in the meridional direction from the Kola Peninsula to the western extremity of the Franz Josef Land Archipelago (Fig. 5). The basement surface along this geotraverse is characterized by a complex structure with uplifts and troughs, which is determined by its strike across the main near-latitudinal structural elements of the Barents Plate. As can be seen from Fig. 5, the variation of sedimentary cover thickness amounts to 10–11 km, thus explaining the notable variations in the geothermal gradient in subsided and uplifted areas, which amounts to ~16 mK/m in the depth interval of 5–10 km and ranges from 24 to 19 mK/m in the depth interval of 0–5 km.

Relatively high heat flow is recorded in the wells located along Profile 4–4 and at sound stations. For example, two wells drilled on the northern slope of the Kil'din Trough yielded 109 and 114 mW/m², while the background heat flow in the central part of the Svalbard Plate is estimated at 76–79 mW/m². The causes of the elevated heat flow in this area were discussed above. At present, it is difficult to give preference to the models related either to the higher activity of the asthenosphere closer to the North Atlantic spreading center or to the secondary rifting that started since the Late Paleozoic.

Let us pass to the characteristic of the thermal field along meridional Trans-Barents Sea geotraverse 7–7. Near the Kola Peninsula, it starts to extend up to the latitude of Franz Josef Land.

This geotraverse is characterized by strong perturbation of isotherms at the transition from the Kola-Kanin Homocline to the South Barents Syncline (Fig. 6). This perturbation is determined by two factors: (1) the average thermal conductivity in the syncline is lower than that in the homocline, where the basement is 5–6 km shallower, and (2) a relatively low heat flow in the South Basin Syncline. If the background heat flow along Profile 4–4 is estimated at 76–79 mW/m², its

value in the South Barents Syneclise is 64–68 mW/m². Northward, closer to the Stockmann–Lunin Threshold, the heat flow increases to 72–77 mW/m².

Such a combination of thermophysical characteristics provides a specific pattern in the distribution of isotherms inherent to organic matter catagenesis. These isotherms become sharply shallower (from 8–12 to 4–5 km) during the transition from the Kola–Kanin Homocline to the South Barents Syneclise and subside gradually again to 6.5–7.5 km in the Franz Josef Land area.

The largest gas-condensate fields are localized in the Stockmann–Lunin Threshold, in consistence with the minimal depth of the catagenetic temperature interval.

Profiles 5–5 and 6–6 (Fig. 1) located in the Franz Josef Land area are poorly provided by geothermal measurements. The heat flow was measured only in the Northern, Nagursky, and HEIS wells. The terrestrial heat flow calculated on the basis of these measurements is estimated at 77–80 mW/m² [21]. Nevertheless, we took these results into account when computing the 3D model of thermal field.

3D TEMPERATURE MODELS OF GEOTRAVERSESES

The technique of computing 3D models was described above. Here, we note only that the procedure consists of two stages.

At the first stage, the temperature sections along geotraversees are placed into a three-dimensional plot according to coordinates of their onset, end, and bend points, if there are any. In addition, the modeling accuracy is estimated at this stage by comparison of calculated and measured temperatures at intersections of profiles. The least squares method, which was applied to estimate the modeling accuracy, shows that discrepancy between depths of the same isotherms is ~100 m, i.e., 0.7% of the total modeling depth, which equals 15 km. We regard this uncertainty as admissible.

At the second stage, with the use of 2D temperature ranges as boundary conditions, the 3D volumetric interpolation is carried out. The less the distance between profiles, the higher the accuracy of the interpolation procedure. In our previous 3D models for the Barents–Kara region, we used as many as 123 geotraversees characterized by CMP and DSS profiling data [8, 9, 18–20]. However, the modeling technique used in this work differs from the previous one by the detailed analysis of the geological situation based on drilling results. Therefore, we developed the model by using only the seven above-mentioned geotraversees. It is particularly noteworthy to compare models of the first and second gen-

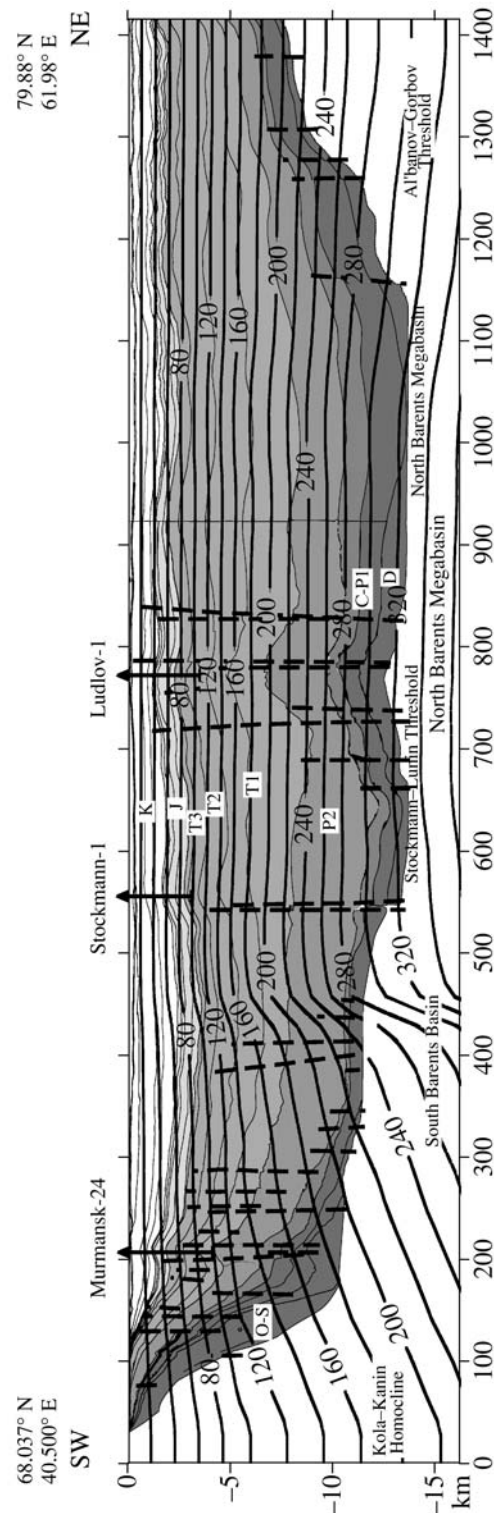


Fig. 6. Geological and geothermal section along Profile 7–7. See Fig. 1 for the profile location and Fig. 2 for legend.

erations and to ascertain the factors responsible for their differences, if any exists.

The 3D models compiled using the technique considered above are quite adequate for tomographic mod-

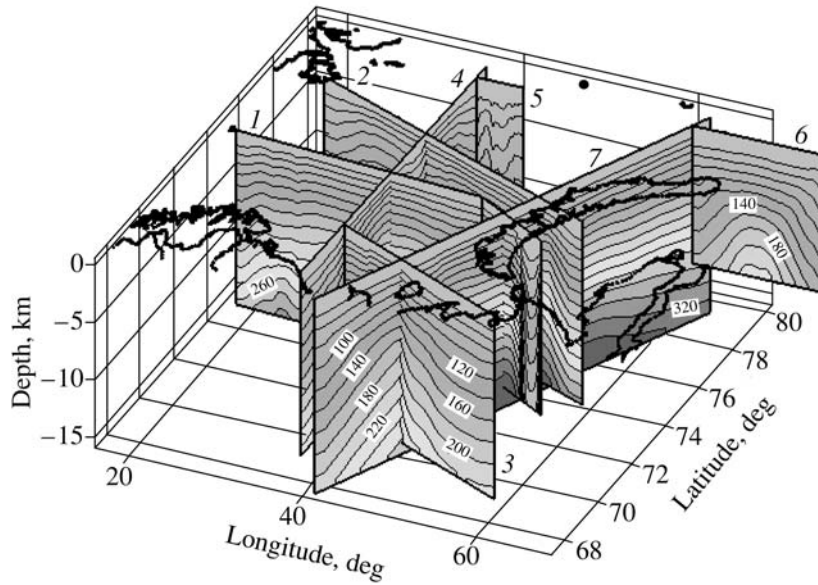


Fig. 7. Temperature sections placed on a 3D plot. See text for explanations. Numerals correspond to numbers of profiles.

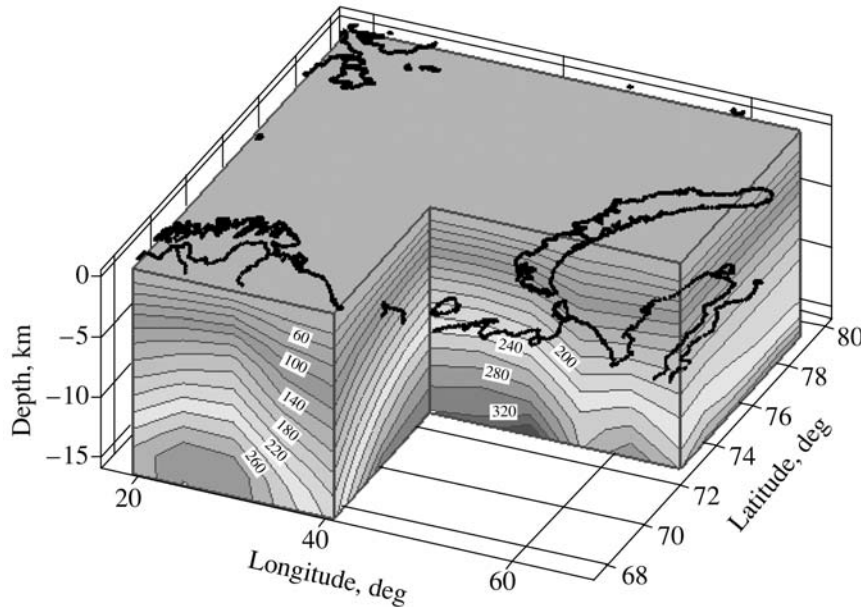


Fig. 8. A 3D model of the temperature field. Isotherms, °C.

els of other geophysical fields or even for the models created in other natural sciences [7, 13, 22–24]. Thus, in this work we substantiate the results of tomographic modeling of the geothermal field, i.e., develop the so-called thermotomographic method.

The method consists in determination of the deep temperature and heat flow density at different depths in coordinates *XYZ*. For real geological objects, this approach implies the temperature distribution depending on the latitude, longitude, and depth. Thus, the 3D thermotomographic model differs from the temperature section because it allows us to glance beyond the

profile line, and this opportunity is particularly important when we are dealing with isometric or mosaic structural elements. Using the respective software, one can easily either compile maps of temperatures (heat flows) for selected depths, show the configuration of isothermal surfaces, or compile the geothermal section in any direction. The thermotomographic maps offer an opportunity to consider the temperature distribution at any depth within the modeling region and to compare the thermal field with geological and geophysical features established independently.

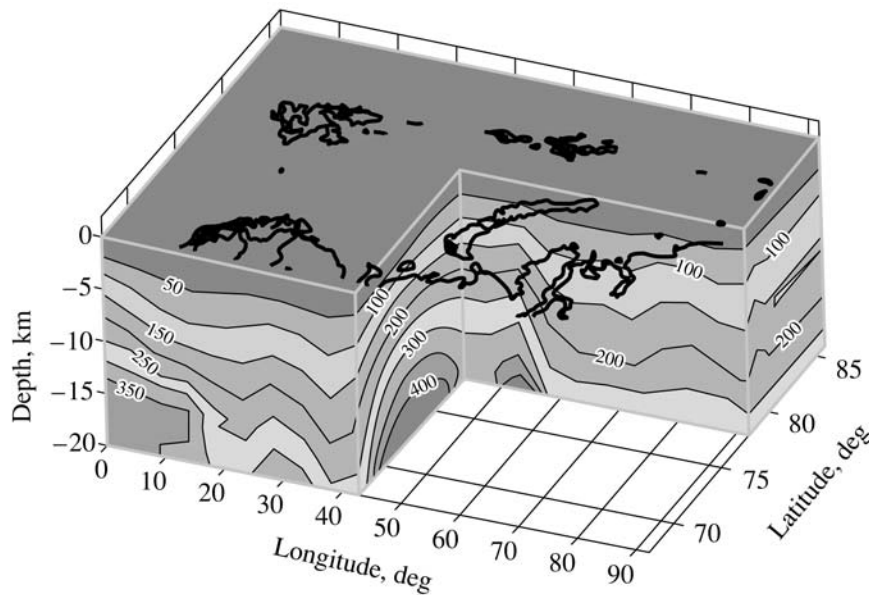


Fig. 9. A 3D model of the temperature field based on interpretation of seismic geotraverses.

The results obtained at the first stage of 3D modeling—allocation of temperature ranges in the 3D plot—are shown in Fig. 7. For implementation of this procedure, a special original computer program that takes into account the depth and position of each profile and transforms initial data of 2D modeling into the TECPLOT format was used.

Volumetric interpolation resulted in obtainment of the model of the temperature field, which makes it possible to determine a temperature in any point of 3D space (Fig. 8). A special blanking in this figure shows temperature domes beneath the South Barents Syncline and the Pechora–Barents Zone of buried uplifts. The dome extends to the South Kara Basin, where it looks autonomously because of the temperature screen beneath Novaya Zemlya. In fact, the formation of both domes has the same cause, namely, the occurrence of thick and low-conductivity sediments and the respective increase in the geothermal gradient within this zone. Northward, in the Stockmann–Lunin area and the North Barents Basin, this effect is enhanced by the local increase in the terrestrial heat flow. The latter factor determines the appearance of another temperature dome in the western part of the region at the edge of the Norwegian shelf, where the sedimentary cover is relatively thin, but the heat flow is slightly higher in comparison with the background level established for the Barents Plate.

Gas and gas-condensate fields discovered in the southeastern part of the Barents Sea and South Kara Basin are localized above the temperature dome. Previously, we pointed out that the Stockmann, Ludlov, Ledovy, North Murmansk, Rusanov, and Leningrad fields are confined to the apical part of the temperature dome [19]. This character of localization can probably

be used as an additional criterion for forecasting the petroleum resource potential. It should be noted that the spatial relations of hydrocarbon fields to temperatures domes was established in the North Caspian and Terek–Caspian sedimentary basins [17]. To compare 3D geothermal field models of the first and second generations, we present in Fig. 9 a model [19] based on seismic surveying along the network of geotraverses that were carried out previously by scientific teams from the Polar Marine Geological Exploration Expedition, the All-Russia Research Institute of Geology and Mineral Resources of the World Ocean [10], Sevmorgeo State Research Enterprise, and other organizations. In terms of the main points, these models are identical; they differ only in some insignificant details. Thus, the implication is that these models are based on the real thermophysical structure and valid boundary conditions.

CONCLUSIONS

- (1) The geothermal field of such isometric regions as the Barents Sea Basin can be reliably depicted only in 3D geometry. This technique offers an opportunity to estimate both lateral and vertical variations of the thermal field.
- (2) Temperature and heat-flow anomalies are formed as a result of nonstationary distribution of heat sources and structural and thermophysical heterogeneities determined by lithological and tectonic factors.
- (3) The thermotomographic analysis of petroliferous basins has shown that economic accumulations of hydrocarbons are localized above zones of rising isotherms, or thermal domes, that were outlined for the first time by 3D modeling of the geothermal field in the eastern Barents Sea and the southern Kara Sea.

ACKNOWLEDGMENTS

This study was supported by the Russian Foundation for Basic Research (project no. 05-05-64011) and the Ministry of Education and Science of the Russian Federation (under the program Development of Scientific Potential of the Higher School).

REFERENCES

1. M. L. Verba and N. V. Sharov, *The State of the Art and Main Problems of the Deep Structure of the Barents Sea Region* (Geol. Inst., Kola Sci. Center, Russian Acad. Sci., Apatity, 1998), Vol. 1, pp. 1–41 [in Russian].
2. E. V. Verzhbitsky, “Geothermal Regime, Seafloor Tectonics, and Hydrocarbon Generation Temperatures in the Eastern Part of the Barents Sea,” *Geotektonika* **36** (1), 86–96 (2002) [*Geotectonics* **36** (1), 76–85 (2002)].
3. *State Geological Map of the Russian Federation, Scale 1 : 1000000 (New Series), Map Sheet R-38-40 (Kolguev). Explanatory Notes*, Ed. by B. G. Lopatin (VSEGEI, St. Petersburg, 2003) [in Russian].
4. I. S. Gramberg, O. I. Suprunenko, K. G. Viskunova, et al., “Petroleum Resource Potential of the West Arctic Shelf of Russia (Hydrocarbon Systems, Resources, and Line of Exploration),” in *Proceedings of All-Russian Conference on 300 Years of the Russian Geological Survey* (St. Petersburg, 2001), Book 3, pp. 30–31 [in Russian].
5. V. G. Levashkevich, Doctoral Dissertation in Geology and Mineralogy (Moscow, 2005).
6. *Methodological and Experimental Principles of Geothermometry* (Nauka, Moscow, 1983) [in Russian].
7. A. V. Nikolaev, “Problems of Geological Tomography,” in *Problems of Geological Tomography* (Nauka, Moscow, 1997), pp. 4–38 [in Russian].
8. L. V. Podgornykh and M. D. Khutorskoi, “Thermal Evolution of the Lithosphere at the Junction of the Baltic Shield and the Barents Sea Plate,” *Izv. Ross. Akad. Nauk, Fiz. Zemli* **34** (3), 56–65 (1998) [*Izv. Physics Solid Earth* **34** (3), (1998)].
9. L. V. Podgornykh, M. D. Khutorskoi, I. S. Gramberg, and Yu. G. Leonov, “A Geothermal 3D Model of the Kara Sea Shelf and Forecast for Its Petroleum Potential,” *Dokl. Akad. Nauk* **380** (2), 333–338 (2001) [*Dokl. Earth Sci.* **380** (7), 782–786 (2001)].
10. V. A. Poselov, A. D. Pavlenkin, and V. V. Butsenko, “Structure of the Lithosphere as Based on DSS Geotraverses in the Arctic,” in *Geologic and Geophysical Characteristics of the Arctic Lithosphere* (VNIIOkeanogeologiya, St. Petersburg, 1996), No. 1, Part 2, pp. 145–155 [in Russian].
11. A. A. Smyslov, U. I. Moiseenko, and T. I. Chadovich, *Thermal Regime and Radioactivity of the Earth* (Nedra, Leningrad, 1979) [in Russian].
12. V. V. Suetnov and E. A. Nikul’shina, “Results of Studying the Parameters of a Neutral Layer in Bottom Sediments of the Southern Barents Sea,” in *Geothermal Studies on Seafloor* (Nauka, Moscow, 1988), pp. 128–134 [in Russian].
13. Yu. A. Tarakanov, “Gravitational Tomography,” in *Problems of Geological Tomography* (Nauka, Moscow, 1997), pp. 236–265 [in Russian].
14. N. V. Ustinov and I. E. Pokrovskaya, “The Upper Jurassic Black Shales of the Barents Sea Shelf,” in *Geological Structure and Petroleum Resource Potential of Arctic Seas of Russia* (VNIIOkeanologiya, St. Petersburg, 1994), pp. 19–29 [in Russian].
15. V. I. Ustritsky and A. N. Khramov, “Geological History of the Arctic in Terms of Plate Tectonics,” in *Seas of the Soviet Arctic* (Nedra, Leningrad, 1984), pp. 253–265 [in Russian].
16. M. D. Khutorskoi, *Geothermometry of the Central Asian Foldbelt* (RUDN, Moscow, 1996) [in Russian].
17. M. D. Khutorskoi, M. P. Antipov, Yu. A. Volozh, and B. G. Polyak, “Temperature Field and a 3D Geothermal Model of the North Caspian Basin,” *Geotektonika* **38** (1), 63–73 (2004) [*Geotectonics* **38** (1), 53–60 (2004)].
18. M. D. Khutorskoi, L. V. Podgornykh, and V. R. Akhmedzyanov, “Geothermal Field and Thermal Evolution of the Lithosphere in the Barents Sea Region,” *Vestn. Ross. Akad. Estestv. Nauk*, No. 5, 55–77 (2000).
19. M. D. Khutorskoi, L. V. Podgornykh, I. S. Gramberg, and Yu. G. Leonov, “Thermal Tomography of the West Arctic Basin,” *Geotektonika* **37** (3), 79–96 (2003) [*Geotectonics* **37** (3), 245–261 (2003)].
20. M. D. Khutorskoi and L. V. Podgornykh, “A 3D Geothermal Model of the Barents Sea Region,” *Dokl. Akad. Nauk* **377** (1), 265–269 (2001) [*Dokl. Earth Sci.* **377** (2), 238–242 (2001)].
21. L. A. Tsybulya and V. G. Levashkevich, *Thermal Field of the Barents Sea Region* (Inst. Geol., Kola Sci. Center, Russian Acad. Sci., Apatity, 1992) [in Russian].
22. A. M. Dziewonski, “Mapping the Lower Mantle: Determination of Lateral Heterogeneity in P-Velocity up to Degree and Order 6,” *J. Geophys. Res.* **89**, 5929–5952 (1984).
23. A. M. Dziewonski and D. L. Anderson, “Seismic Tomography of the Earth’s Interior,” *Amer. J. Sci.* **72** (5), 483–494 (1984).
24. *Seismic Tomography: Theory and Practice*, Ed. by H. M. Iyer and K. Hirahara (London, 1993) pp. 519–584.

Reviewers: A.O. Gliko and E.V. Shipilov